buildings

MDPI

Article

Seismic Response Comparisons of Prefabricated and Cast In Situ Subway Station Structures in Liquefiable Site

Junhai An, Qiaofeng Liu, Yanhua Zhang and Xuehui Zhang *

School of Civil Engineering, Hebei University of Science and Technology, Shijiazhuang 050018, China; tsanjunhai@126.com (J.A.); lqf103121@126.com (Q.L.); zhangyanhua0131@163.com (Y.Z.)
* Correspondence: zhxuehui@hebust.edu.cn; Tel.: +86-178-5433-9501

Abstract: Based on the engineering practice of the first prefabricated subway station (Shuangfeng Station) in Changchun, China, the applicability of prefabricated subway station structures (PSSSs) in liquefiable sites in seismically defended areas is investigated. In this paper, the finite difference software FLAC3D 5.0 is used to carry out the seismic response analysis of the PSSS in liquefiable ground, and the calculation results of the PSSS are compared with those of the same type of cast-in-place subway station condition. The results show that the trend of foundation excess pore pressure ratio (EPPR) in the PSSS condition is similar to that of the cast-in-place condition. For different ground vibration inputs, there is not much difference between the PSSS and the cast-in-place structure on the pore pressure (PP) of the surrounding liquefiable soil. The acceleration response of the PSSS is slightly smaller than that of the cast-in-place structure, and it has a better ability to adapt to ground deformation. The deformation of the upper part of the PSSS is slightly larger than that of the lower part, which is an important part of its deformation control, and the middle part is the key part of its strength control due to the presence of the center plate, which results in a significant increase in stiffness and stress. The flexible connection of the PSSS is easier to adapt to a larger vertical deformation than rigid connection, and its ability to resist overturning is better. Under the premise of ensuring static waterproofing, the PSSS can be constructed in liquefiable sites in earthquake-proof areas.

Keywords: prefabricated subway station structure; liquefaction; seismic response; adaptability to deformation; numerical simulation

check for updates

Citation: An, J.; Liu, Q.; Zhang, Y.; Zhang, X. Seismic Response Comparisons of Prefabricated and Cast In Situ Subway Station Structures in Liquefiable Site. *Buildings* **2023**, *13*, 3071. https://doi.org/10.3390/buildings13123071

Academic Editor: Piero Colajanni

Received: 12 November 2023
Revised: 29 November 2023
Accepted: 7 December 2023
Published: 9 December 2023

1. Introduction

Prefabricated subway station structure (PSSS) construction technology is an important way to realize the industrialization of large-scale urban underground engineering construction and construction mechanization, and it is an important initiative to promote the realization of the Chinese-style modernization of the green, intelligent, and low-carbon building scene. It is favorable for accelerating the construction speed, ensuring the quality of the project, reducing environmental pollution, reducing the cost of the project, and solving the problem of winter construction in the cold region [1]. Yang Xiuren [2] firstly proposed the construction concept of using full prefabricated technology to build open-cut subway stations and successfully put it into practice in some stations of the Changchun Metro Line 2. Nowadays, PSSSs are quietly leading the development direction of subway engineering construction and research. However, compared with the cast-in-place structure as a rigid structural system, the PSSS is a flexible structural system made of independent prefabricated components and their tongue-and-groove nodes. The two structures are obviously different in terms of structural form, member connection, force characteristics, construction technology, etc., and their seismic response and seismic performance must also be significantly different. Therefore, the seismic design of a PSSS should not directly follow the research data and conclusions of existing cast-in-place structures.

In recent years, related scholars have carried out a series of studies on the seismic performance of PSSSs. TAO et al. [3] investigated the seismic response of a PSSS based on shaking table tests. The results show that it will undergo severe damage and may degrade to a three-hinged arch mechanism under rarefied seismic actions. Hongtao Liu and Xiuli Du [4,5] carried out tests on the damage pattern and mechanical properties of prefabricated station members in the sleeve connection zone under seismic action. The results show that there is an obvious stiff domain effect in the grouting sleeve region, and the cracks after the damage of the specimen are mainly distributed at the end of the sleeve. Using Abaqus software, Ding Peng, Tao Lianjin et al. [6,7] analyzed the seismic performance of a PSSS under the conditions of various site categories. The results of the study show that a PSSS has a better seismic performance than a cast-in-place structure under the seismic action of the fortification. Based on numerical simulation, Jiang et al. [8] investigated the distinction between fully prefabricated and homogeneous cast-in-place station structures in terms of deformation, internal force, and damage under the eight-degree-zone fortification, rarefied and very rarefied earthquakes. Fenghao Wu [9] systematically studied the elastic–plastic response of a PSSS using tongue-and-groove grouted joints and gave the damage sequence of the joints under strong earthquakes. The above research results reveal the seismic deformation mode and destructive mechanism for PSSSs from different angles, which provide theoretical support to the seismic design for structures. Jinnan Chen et al. [10,11] studied the seismic performance and seismic vulnerability analysis of a PSSS. The study shows that the upper column end of the PSSS is the weakest part of the structure. Prefabricated subway station structures are less vulnerable to damage than cast-in-place subway station structures. Chunyu Wu et al. [12] modeled a partially prefabricated subway station with different connection forms and comparatively investigated its behavior under three kinds of seismic actions. Lingvay Iosif et al. [13] investigated that the synergistic effect of the internal factors of complex soil environments and interfering electromagnetic fields can accelerate the corrosion damage of underground structures. Adverse stratigraphic environments at liquefiable sites may significantly affect the seismic performance of subsurface structures. However, all these studies place the PSSS in the general stratum and do not consider the influence of the liquefiable stratum. Existing studies have shown that large soil deformations caused by seismic liquefaction are the most important external factor in the occurrence of damage to underground structures [14].

Along with the rapid development of city railway transportation, an increasing number of subway structures would inevitably cross liquefied soil layers. Over 60% of the rail transit lines in Taiyuan, China, run through soil layers that are prone to liquefaction. These layers of liquefied soil are mostly found above the structural floor slabs in subway stations. The majority of these layers are mildly to moderately liquefied, with localized severe liquefaction [15–17], see Figure 1. At present, the research on the seismic response characteristics and damage mechanism of PSSSs in liquefiable strata has not yet been published, which poses a great challenge for its further popularization and application in different strata.

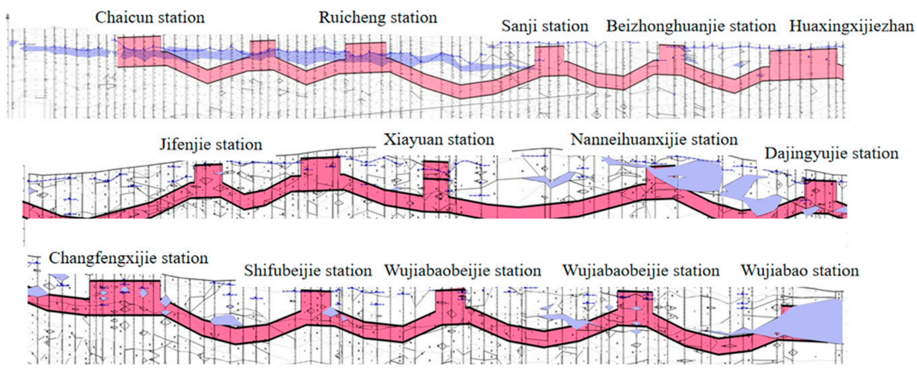

Figure 1. Liquefiable stratigraphic distribution in Taiyuan Metro, China.

Therefore, this paper relies on the actual Changchun Shuangfeng Station project and considers placing it in the liquefiable stratum. The finite difference software FLAC3D5.0 is used to develop a numerical analysis model for the structural dynamic interaction of soil–PSSS. An in-depth revelation of the seismic response of PSSSs in the liquefiable strata is presented to provide valuable references for their further engineering applications.

2. Project Overview

Changchun Metro Shuangfeng Station is an underground two-story single-arch, large-span PSSS, which was constructed by the pile+anchor system open-cut method. The station structure is 20.5 m wide and 17.45 m high, and the main body of the station frame is divided into 2 m rings vertically, with a center column for every three rings, and a ring is composed of seven prefabricated components. The method of joining the members to each other is mortise–tenon, and the joints are sealed by injecting epoxy resin into the joint gaps. The center plate, center column, and bottom beam of the station are all post-cast members, and the detailed structural dimensions are shown in references [18,19]. Figure 2 gives the structural section of the PSSS.

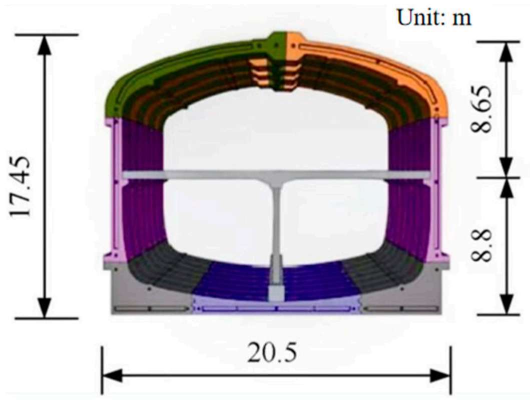

Figure 2. Section diagram of PSSS.

3. Numerical Modeling of Soil–Structure Interaction System

3.1. Numerical Models

Based on the Changchun Shuangfeng subway station, FLAC3D software is used to establish the numerical analysis model of the soil–underground structure interaction. The size of the model is 160 m × 46 m × 20 m, and the depth of the structure is 3 m. The maximum size of the model grid is 1 m and the minimum size is 0.2 m. The soil layer where the structure is located is a liquefiable soil layer. Fixed constraints are used at the bottom of the model boundary in the dynamics calculations, and free-field boundary conditions are imposed around the model. Figure 3 shows the numerical calculation model.

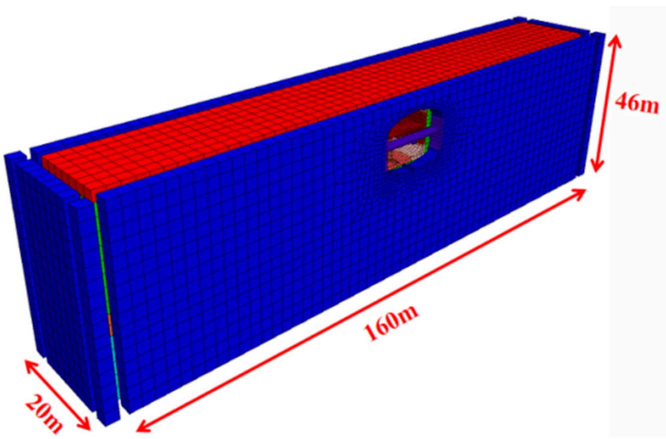

Figure 3. Soil–underground structure dynamic interaction model.

The structural section of the subway station is 20.5 m long and 17.45 m wide, and the structural profile consists of seven prefabricated components of five categories, numbered A, B (1–2), C (1–2), D, and E, with mortise and tenon joints at each prefabricated node. After the prefabrication of the outer contour of the structure, the center plate and center column of the structure were poured with concrete. The thickness of the center plate is 400 mm, and the cross-section size of the center column is 500 mm × 500 mm. Figure 4a shows the structure of the PSSS. Figure 4b shows the same type of cast-in-place subway station structure model.

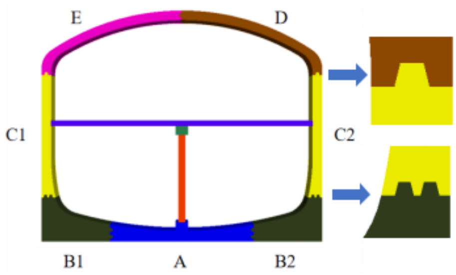

(**a**)

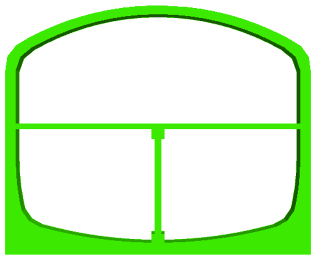

(**b**)

Figure 4. Improved response displacement method model. (**a**) Prefabricated structure; (**b**) cast-in-place structure.

Figure 5 shows a sketch of the model and the arrangement of the monitoring points. The meanings of the letters in Figure 5b are acceleration A, pore pressure P, wall monitoring point Q, and bottom plate monitoring point B, respectively.

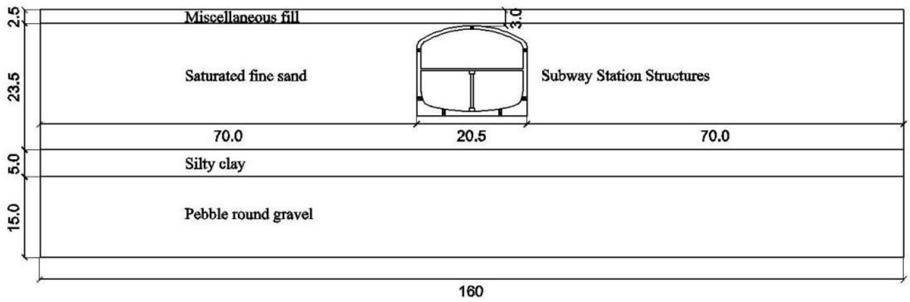

(**a**)

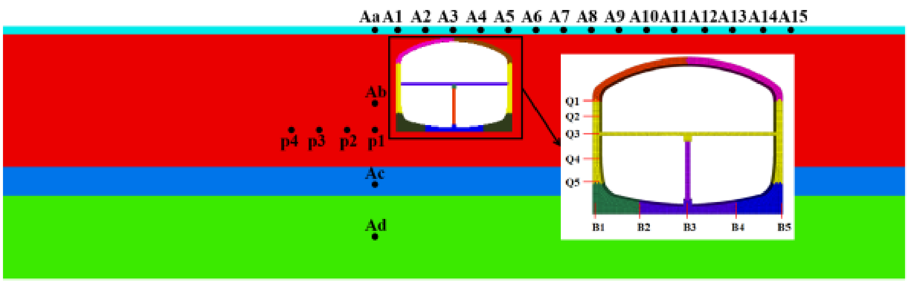

(**b**)

Figure 5. Model sketch and monitoring point arrangement. (**a**) Distribution of soil layers and location of structures; (**b**) monitoring point layout.

3.2. Site Conditions and Parameter Selection

In the computational model, the Mohr–Coulomb constitutive model was chosen for the miscellaneous fill, clay, and pebbles. The soil layer where the subway station structure is located is selected to be a saturated fine sand soil layer. The saturated fine sand soil layer was modeled using the PL-finn model in FLAC3D. The distribution of soil layers and their physico–mechanical parameters are shown in Table 1. An isotropic elastic model is chosen for the constitutive model of the subway station structure. The damping of the structure adopts local damping, and the damping coefficient is 0.172 (damping ratio is 5%). The physical and mechanical parameters of each member of the structure are shown in Table 2.

Table 1. Physical and mechanical parameters of site soil layer.

Soil Types	Soil Thickness	Natural Density ρ (g/cm^3)	Volume Modulus K (Pa)	Shear Modulus G (Pa)	Poisson Ratio γ	Cohesion C (kPa)	Friction Angle φ (°)
① Miscellaneous fill	2.5	1.90	3×10^7	1×10^7	0.35	5	25
② Saturated fine sand	23.5	1.80	2×10^7	7×10^6	0.30	0	35
③ Silty clay	5.0	2.00	2.65×10^7	1.52×10^7	0.28	25	10.5
④ Pebble round gravel	15.0	2.10	3×10^8	2×10^8	0.22	0	35

Table 2. Physical and mechanical parameters of concrete.

Structural Types	Concrete Strength Grade	Elastic Modulus G (GPa)	Density ρ (Kg/m^3)	Computational Model	Poisson Ratio γ
beam	C40	32.5	2500	Elastic	0.20
stele	C45	33.5	2500	Elastic	0.18
wall	C40	32.5	2500	Elastic	0.20

3.3. Contact Surface Settings

The contact surfaces are established at the joints between the prefabricated components, and the contact surfaces are set up using the guide-to-guide method in the FLAC3D software. The contact surfaces of the structural nodes of the prefabricated subway station are shown in Figure 6. The normal stiffness kn and tangential stiffness ks of the contact surface are calculated by Equation (1).

$$k_n = k_s = 10 \max\left[\frac{\left(K + \frac{4}{3}G\right)}{\Delta z_{\min}}\right] \tag{1}$$

where

K—bulk modulus

G—shear modulus

$\Delta Z_{\min}$—the minimum size on the connection region in the direction normal to the contact surface.

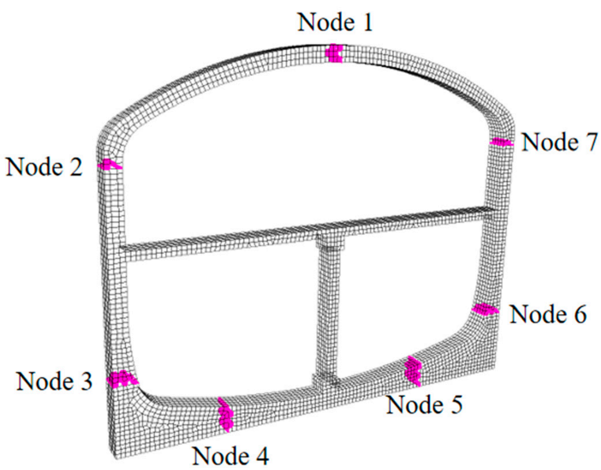

Figure 6. Schematic diagram of contact surface.

The contact surface parameters, as shown in Table 3.

Table 3. Prefabricated node contact surface unit parameters.

Typology	Normal Stiffness (Pa/m)	Shear Stiffness (Pa/m)	Cohesion (kPa)	Internal Friction Angle
Contact surface	1.67×10^{12}	1.67×10^{12}	10	15

3.4. Input Ground Motion

The seismic waves were selected to be Changchun artificial wave, Kobe wave, and EL-Centro wave with different spectral characteristics. The peak accelerations of the seismic waves were adjusted to 0.15 g, 0.25 g, and 0.4 g. Horizontal ground shaking was input from the bottom of the bedrock, and the holding time was 30 s. The acceleration time curves and Fourier spectra of the three seismic waves are shown in Figures 7 and 8.

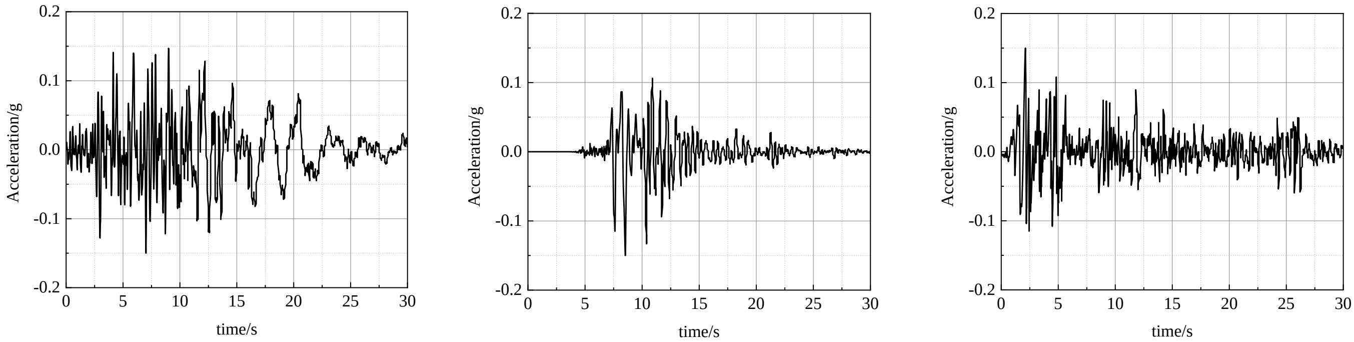

(**a**) Changchun artificial wave (**b**) Kobe wave (**c**) EL-Centro wave

Figure 7. Input seismic wave time-history curve.

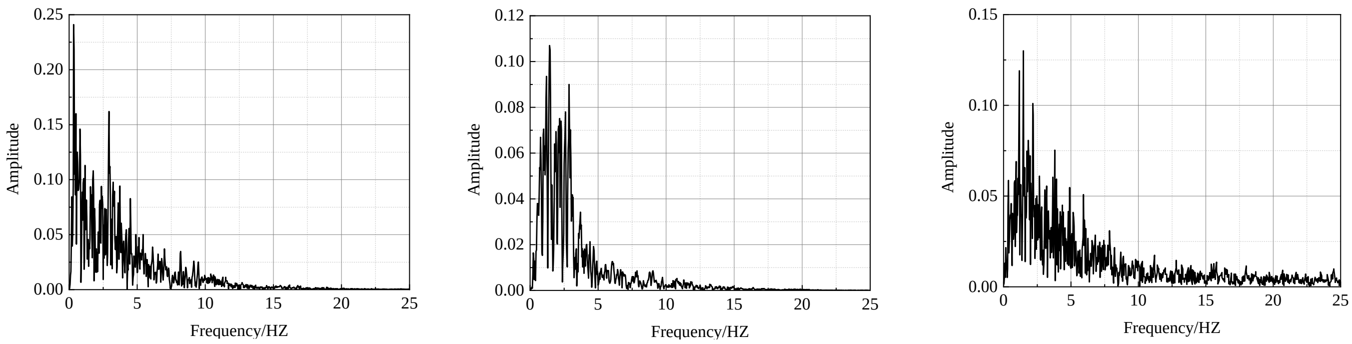

(**a**) Changchun artificial wave (**b**) Kobe wave (**c**) EL-Centro wave

Figure 8. Fourier spectrum of input seismic wave.

4. Seismic Response Analysis of Strata

4.1. Analysis of Pore Pressure (PP) Evolution

Figures 9–11 show the time-history curve of the excess pore pressure ratio (EPPR) at the monitoring point of 5 m (P1), 10 m (P2), 15 m (P3), and 20 m (P4) from the left side of the structural base plate of the PSSS under the effect of ground motion with different peak accelerations. As seen in Figures 9–11, the EPPR shows the development course of "slow increase at the beginning, followed by a rapid rise and finally stabilized". However, the soil EPPR varies greatly under different ground shaking. This is determined by the different spectral characteristics of the seismic waves. During the initial phase of the ground shaking action, a small amount of negative PP occurs in the soil. This is due to a small amount of shear swelling occurring in the soil. When 0.15 g and 0.25 g seismic waves are input, there is no obvious pattern in the EPPR. When the peak acceleration reaches 0.4 g, the EPPR of the soil layer close to the structure is less than the soil layer away from the structure. This indicates the obvious inhibition of seismic liquefaction by the subsurface structure under strong earthquakes. Among them, the Changchun artificial wave condition has the largest EPPR, the Kobe wave condition is the second, and the EL-Centro wave is the smallest. This indicates that the liquefiable site responds more strongly to seismic waves with medium and high frequency distribution. Therefore, the following analysis of the seismic response results focuses on the calculated data under the action of the Changchun artificial wave.

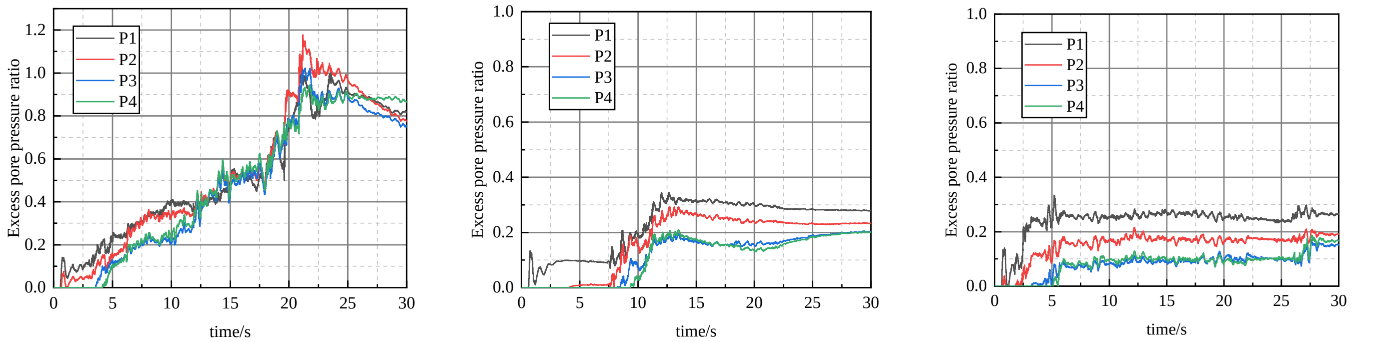

(**a**) Changchun artificial wave (**b**) Kobe wave (**c**) EL-Centro wave

Figure 9. Time-history curve of EPPR under different ground motions (0.15 g prefabricated condition).

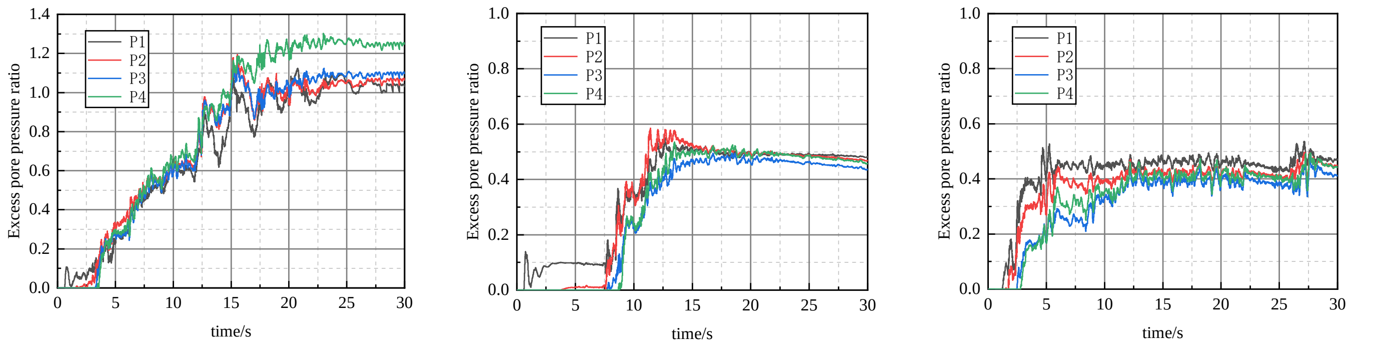

(**a**) Changchun artificial wave (**b**) Kobe wave (**c**) EL-Centro wave

Figure 10. Time-history curve of EPPR under different ground motions (0.25 g prefabricated condition).

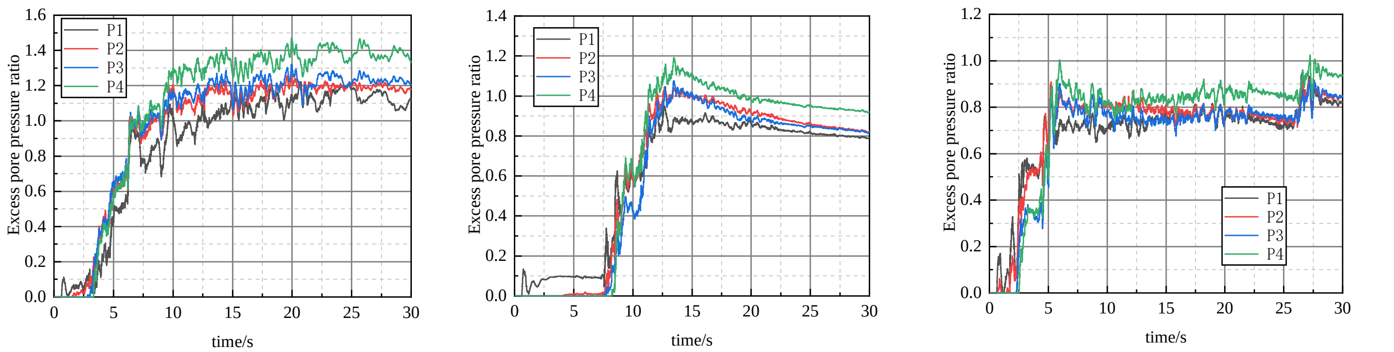

(**a**) Changchun artificial wave (**b**) Kobe wave (**c**) EL-Centro wave

Figure 11. Time-history curve of EPPR under different ground motions (0.4 g prefabricated condition).

In order to compare the difference in the effect of the two structures on the PP of the surrounding liquefiable soil layer, Figures 12 and 13 show the time-history curve of the EPPR. As can be seen from Figures 12 and 13, the trends of the pore water pressure changes in the soil under the two conditions are basically the same. Under 0.15 g ground shaking, only a tiny portion of the soil body liquefied. At this point, the EPPR is slightly greater in the PSSS condition than in the cast-in-place condition, and its PP dissipates more quickly. When the input peak ground acceleration reaches 0.25 g and above, the model foundation is almost completely liquefied. The peak value and variation in the EPPR tend to be the same in the two conditions. This indicates that the difference between the two structures on the pore pressures of the surrounding liquefiable soils is relatively small for different ground shaking inputs, especially for high-intensity seismic wave action. The PSSS built in the high-intensity zone can be applied to liquefiable site conditions under the condition of ensuring static waterproofing.

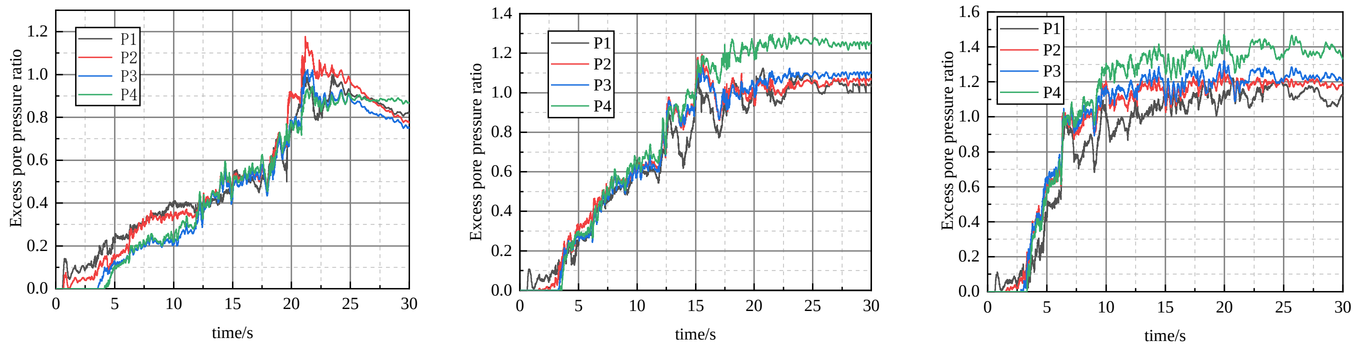

(**a**) 0.15 g (**b**) 0.25 g (**c**) 0.4 g

Figure 12. Time-history curve of EPPR (PSSS condition, Changchun artificial wave condition).

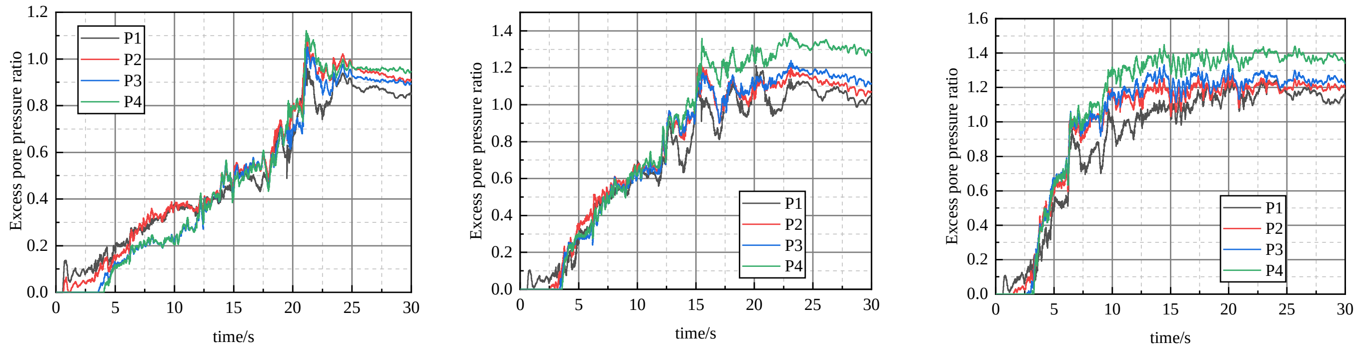

(**a**) 0.15 g (**b**) 0.25 g (**c**) 0.4 g

Figure 13. Time-history curve of EPPR (cast-in-place condition, Changchun artificial wave condition).

4.2. Acceleration Analysis

4.2.1. Peak Surface Acceleration

Figure 14 shows the peak ground acceleration at different monitoring points of the model foundation surface when artificial waves with different peak values of ground shaking are input. In the figure, the left wall of the station structure is taken as the origin and to the right as the positive *X*-axis. As shown in Figure 14, the soil directly above the structure has a significantly smaller acceleration response than the lateral soil for the two structure conditions. As the distance from the underground structure increases, its acceleration also increases gradually, until it reaches about 50 m from the structure, then the acceleration response at the surface stabilizes and decreases. It shows that the structure has a certain seismic isolation of the ground acceleration response. When inputting lower-intensity ground shaking (0.15 g), the peak ground acceleration of the PSSS condition is marginally larger than the cast-in-place condition, especially at the measurement points directly above the station structure. This may be due to the fact that the stiffness of the PSSS is less than that of the cast-in-place structure, resulting in a smaller seismic isolation effect. At this time, the model foundation has not undergone seismic liquefaction and is in the elastic stage; when the input peak ground acceleration reaches 0.25 g and above, the model foundation has undergone obvious seismic liquefaction, and there is not much difference in the ground acceleration between the two conditions.

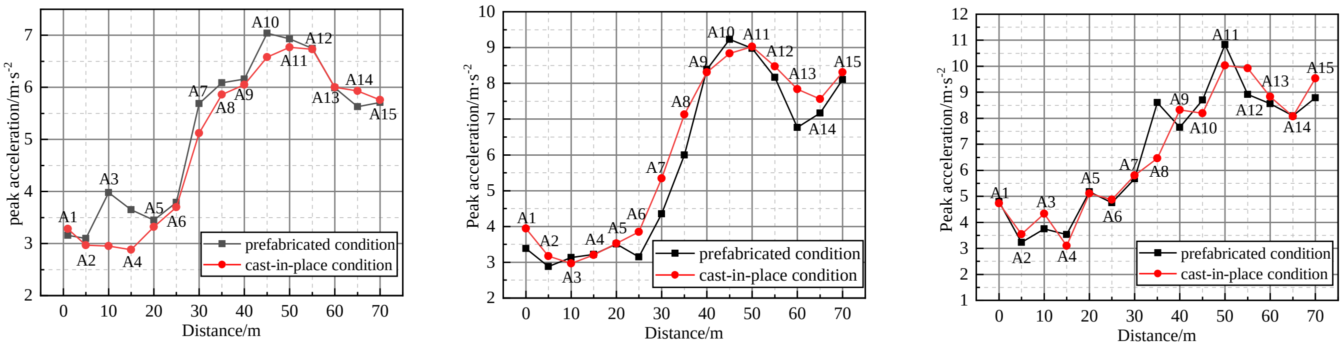

(**a**) 0.15 g (**b**) 0.25 g (**c**) 0.4 g

Figure 14. Peak acceleration of different surface measuring points.

4.2.2. Acceleration Response of Different Soil Layers

Figure 15 shows the acceleration amplification factor curves for the left side of the subway station structure at 5 m in different depths of the soil layer in the prefabricated, cast-in-place, and free-field conditions. In the figure, the point 0 of the vertical axis of the graph is taken to the bottom of the model. As seen in Figure 15, the presence of subsurface structures somewhat reduces the acceleration response of the soil. There is little difference in the difference between the effects of soil acceleration for the two conditions. From bedrock to the ground surface, the two conditions show a tendency of increasing and then decreasing. The higher the input ground vibration intensity, the earlier the location of the acceleration inflection point appears, and the location of the inflection point of the two is also very close to each other. Therefore, the analysis of the acceleration response of the liquefiable site soil and anti-liquefaction measures in the station condition of the PSSS can refer to the data and conclusions of the cast-in-place condition.

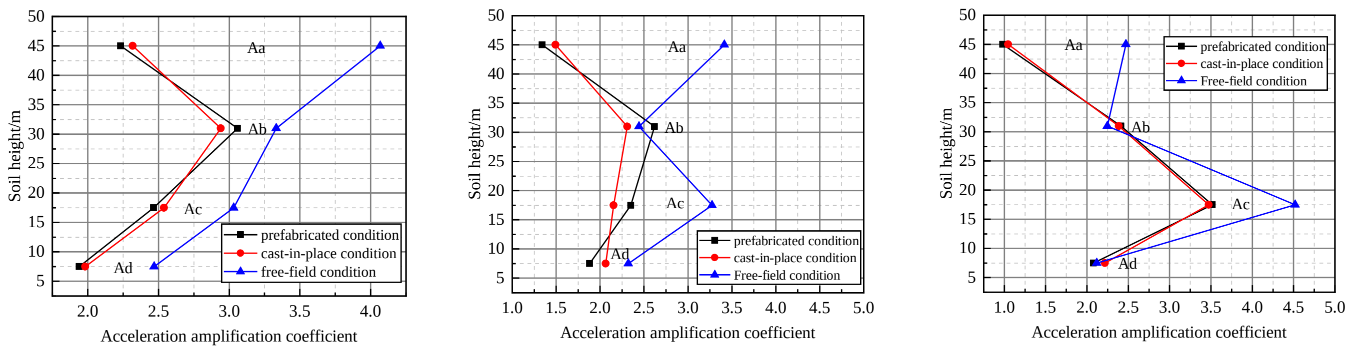

(**a**) 0.15 g (**b**) 0.25 g (**c**) 0.4 g

Figure 15. Amplification coefficient of soil acceleration at different depths.

In the free-field condition, the acceleration response of the soil layer gradually increases from bottom to top when a smaller peak ground shaking acceleration (0.15 g) is input, and at this time, the liquefiable site is in an elastic state; with the increasing strength of the input ground vibration, the liquefaction range of the soil body is gradually extended. The amplification coefficient of the acceleration response of the soil also has an obvious inflection point, and its peak value may appear an extreme phenomenon, and the acceleration response along the depth of the soil layer has no obvious pattern.

5. Seismic Response Analysis of Subway Station Structure

5.1. Acceleration Analysis

Figure 16 shows the peak accelerations at different heights of the side walls of the structure. Among them, the monitoring points Q1, Q3, and Q5 are the connections of the wall (member C1) with member E, center slab, and member B1, respectively. Q2 and Q4 are the locations in the center of the wall (member C1) at each floor, respectively.

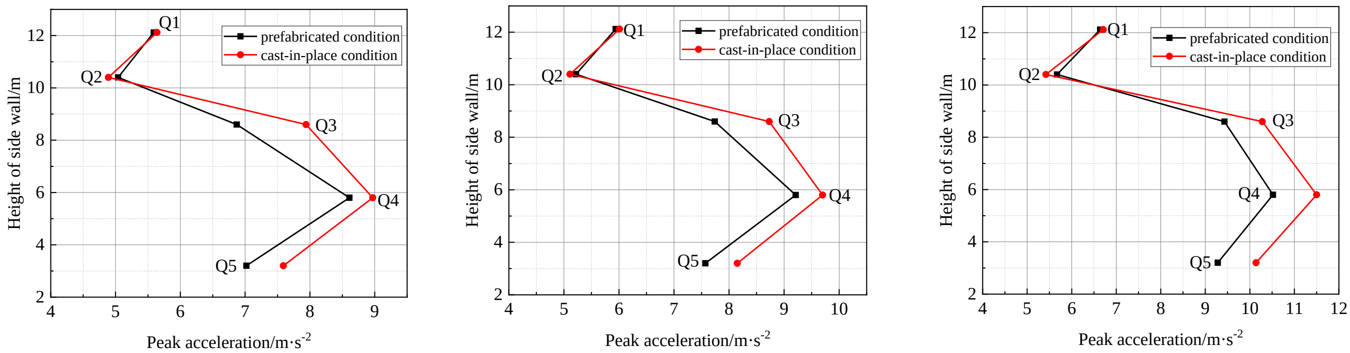

(**a**) 0.15 g (**b**) 0.25 g (**c**) 0.4 g

Figure 16. Peak acceleration of side wall (component C1).

As seen in Figure 16, the acceleration response of the wall gradually increases with an increase in the intensity of the input ground shaking. Overall, the acceleration response of the wall in the underground second floor of the structure is significantly larger than in the underground first floor. In the liquefiable site, the peak acceleration of the wall of the underground first floor of the PSSS differs very little from that of the cast-in-place structure. However, the result is reversed for the underground second floor. This is because the overall stiffness of the PSSS is less than the cast-in-place structure. In conclusion, the acceleration response of the PSSS is smaller than that of the cast-in-place structure. This reflects its applicability in liquefiable sites.

5.2. Structural Stress Analysis of Prefabricated Subway Station

Table 4 gives the amplitude of the principal stress response for the wall of the two structures. As shown in Table 4, when the peak acceleration of the input ground vibration is low, the peak maximum and minimum principal stresses at each measurement point do not differ much for the two conditions. The maximum principal stress amplitude of the cast-in-place structure is significantly greater than that of the PSSS as the intensity of the ground shaking increases. This indicates that the PSSS with flexible connections bears less tensile stress at its nodes and the structure is safer. Among the various monitoring points of the wall, monitoring point Q3 has the highest stress, monitoring point Q1 is the next highest, and monitoring point Q5 has the lowest. This indicates that the deformation of the underground first floor of the structure is slightly greater than the underground second floor, which is an important link in the control of structural deformation. The middle part of the subway station structure is an important part of the structural strength control because of the existence of the center plate, resulting in a significant increase in stiffness and stress, which is the key part of the structural strength control.

Table 4. Main stress response amplitude (MPa) of subway station structure.

Condition		Principal Stress	Q1	Q2	Q3	Q4	Q5
0.15 g	prefabricated	minimum	−2.29	−2.01	−4.24	−3.04	−3.23
		maximum	0.52	0.15	2.11	0.57	0.21
	cast-in-place	minimum	−2.26	−2.02	−4.01	−3.06	−3.13
		maximum	0.72	0.15	1.98	0.58	0.05

Table 4. *Cont.*

Condition		Principal Stress	Q1	Q2	Q3	Q4	Q5
0.25 g	prefabricated	minimum	−2.35	−2.10	−4.74	−3.09	−3.76
		maximum	0.56	0.16	2.36	0.59	0.27
	cast-in-place	minimum	−2.30	−2.10	−4.52	−3.10	−3.54
		maximum	0.77	0.16	2.26	0.60	0.09
0.4 g	prefabricated	minimum	−2.43	−2.15	−4.65	−3.19	−3.81
		maximum	0.56	0.17	2.54	0.70	0.13
	cast-in-place	minimum	−2.33	−2.17	−4.21	−3.22	−3.59
		maximum	0.80	0.17	2.77	0.71	0.28

5.3. Analysis of Lateral Deformation of Prefabricated Subway Station Structure

The time-history curves of the relative inter-story displacements of the two structures under different seismic intensities and the Fourier spectrum of the negative two layers of the structure are shown in Figures 17–19. As shown in the figures, the difference between the time-range curves of the relative displacements between the underground first floor and the underground second floor of the two conditions of the ground vibration input process is very small, and their spectra also almost overlapped. Their deformation amplitude occurrence moments are also basically the same. Only in the second half of the excitation is there a small difference between the leftward and rightward deformations of the two conditions. Therefore, the difference in the overall deformation of the two structures is small. The dynamic characteristics of the PSSS remain suppressed by the constraints of the surrounding strata.

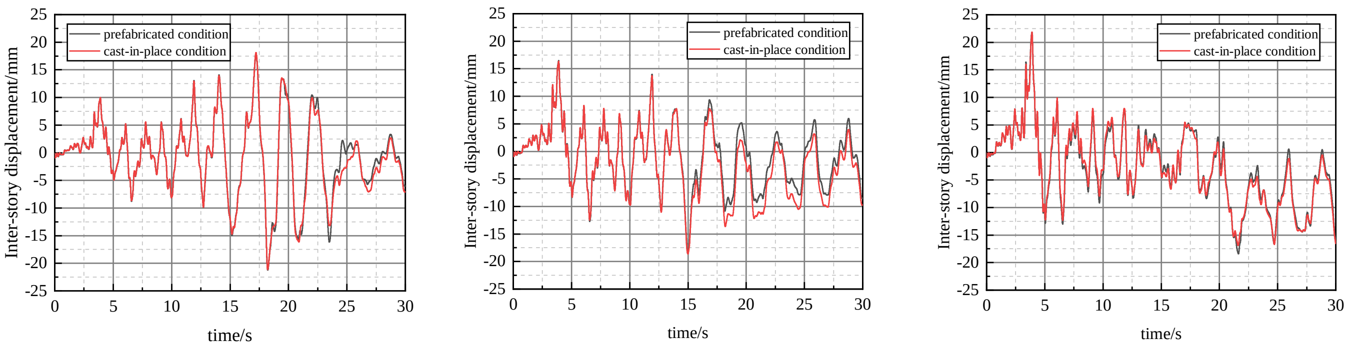

(**a**) 0.15 g (**b**) 0.25 g (**c**) 0.4 g

Figure 17. Time-history curve of inter-story displacement of underground first floor.

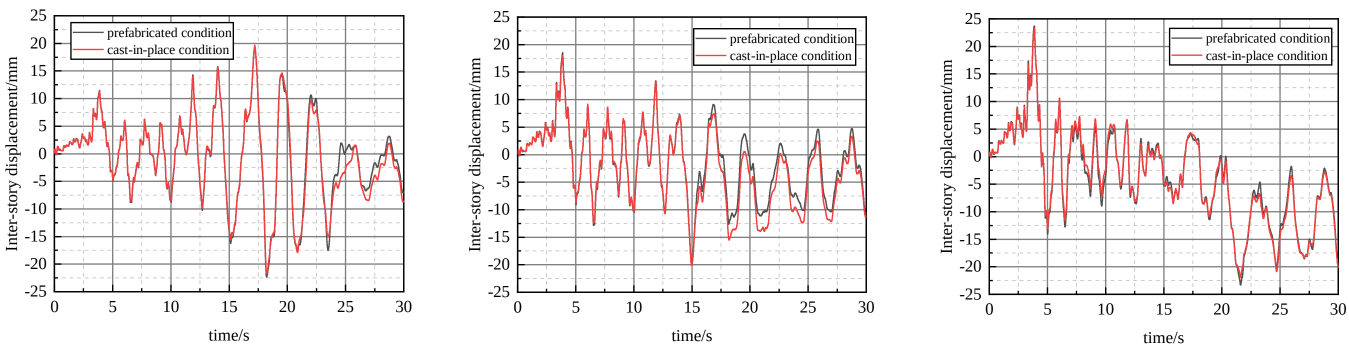

(**a**) 0.15 g (**b**) 0.25 g (**c**) 0.4 g

Figure 18. Time-history curve of inter-story displacement of underground second floor.

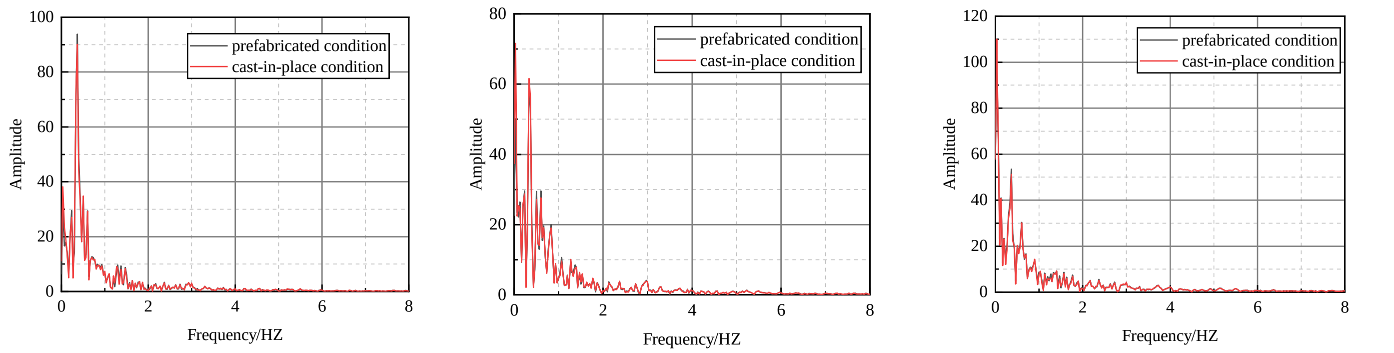

(**a**) 0.15 g (**b**) 0.25 g (**c**) 0.4 g

Figure 19. Fourier spectrum.

Table 5 shows the inter-story displacements and their maximum inter-story displacement angles for the two structural conditions to further analyze the inter-story deformation. Under 0.15 g and 0.25 g ground shaking, the deformation of the underground second floor of the structure is greater than that of the underground first floor for both conditions. This indicates that the structure still undergoes shear-type deformation at this time. However, the maximum inter-story displacement angle of the prefabricated condition is slightly less than that of the cast-in-place condition. This indicates that the PSSS has a better ability to adapt to the ground deformation. Under 0.4 g ground shaking, the difference between the underground first floor and underground second floor of the structure for both conditions is very small. However, the maximum inter-story displacement angle exceeds 1/550, indicating that the structure enters the elastic–plastic state. The structures have similar stratigraphic adaptability after entering the elastic–plastic state for both conditions.

Table 5. Horizontal peak deformation of structure.

Peak Ground Motion Acceleration	Building Floor	Structural Style	Maximum Inter-Story Displacement (mm)	Maximum Inter-Story Displacement Angle
0.15 g	Underground first floor	prefabricated	−5.91	1/1320
		cast-in-place	−6.97	1/1119
	Underground second floor	prefabricated	−6.85	1/1197
		cast-in-place	−8.50	1/965
0.25 g	Underground first floor	prefabricated	−8.42	1/926
		cast-in-place	−9.64	1/809
	Underground second floor	prefabricated	−10.5	1/781
		cast-in-place	−11.02	1/744
0.4 g	Underground first floor	prefabricated	−16.28	1/479
		cast-in-place	−16.62	1/469
	Underground second floor	prefabricated	−20.23	1/405
		cast-in-place	−20.05	1/409

5.4. Floating Analysis of Prefabricated Subway Station Structure

Figures 20 and 21 give the time-course curves of the vertical displacements at various locations of the structural base slab and the structural seismic deformation diagrams. Under the 0.15 g ground shaking, the vertical displacement of the structure shows the development stage of "a small amount of sinking at the beginning, followed by a sharp floating, and finally tends to fall". The cause of the settlement phenomenon is mainly due to the loose soil below the structure, which is densified under the effect of the ground shaking and causes subsidence. When the input ground vibration intensity increases to 0.25 g, the structure exhibits up and down fluctuations around the 0 coordinate axis in the first 12 s time period, then rises sharply and, finally, stabilizes. When the input ground vibration intensity is increased to 0.4 g, the time period of the oscillatory change in the subway station structure further decreases to about 5 s. This indicates that the higher the input ground vibration intensity, the shorter the time for the structure to appear floating and reach its peak value.

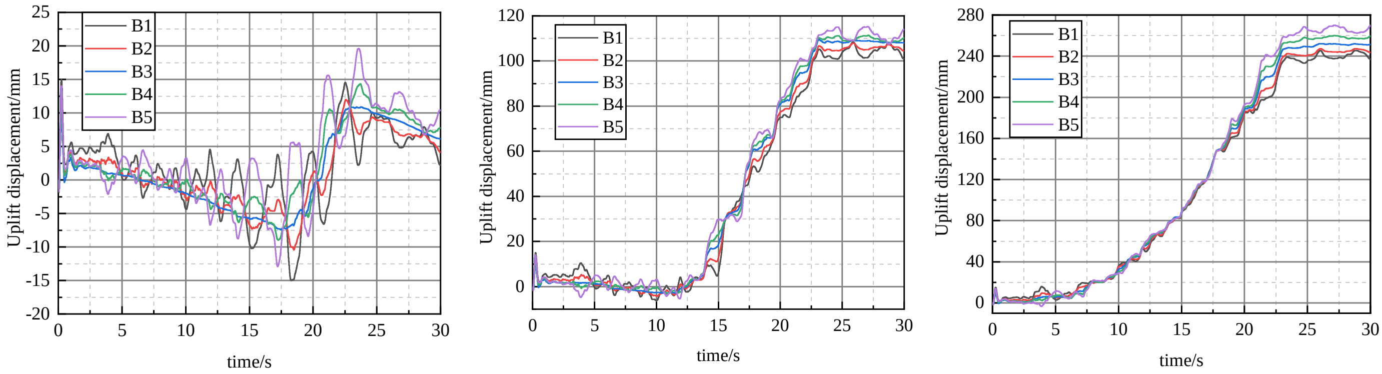

(**a**) 0.15 g (prefabricated) (**b**) 0.25 g (prefabricated) (**c**) 0.4 g (prefabricated)

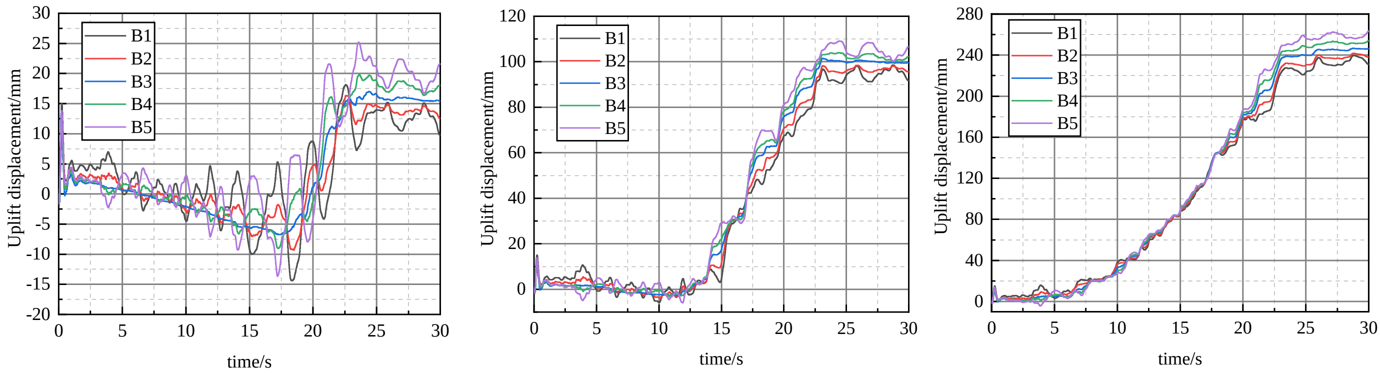

(**d**) 0.15 g (cast-in-place) (**e**) 0.25 g (cast-in-place) (**f**) 0.4 g (cast-in-place)

Figure 20. Floating displacement time-history curves at different positions of the structural floor.

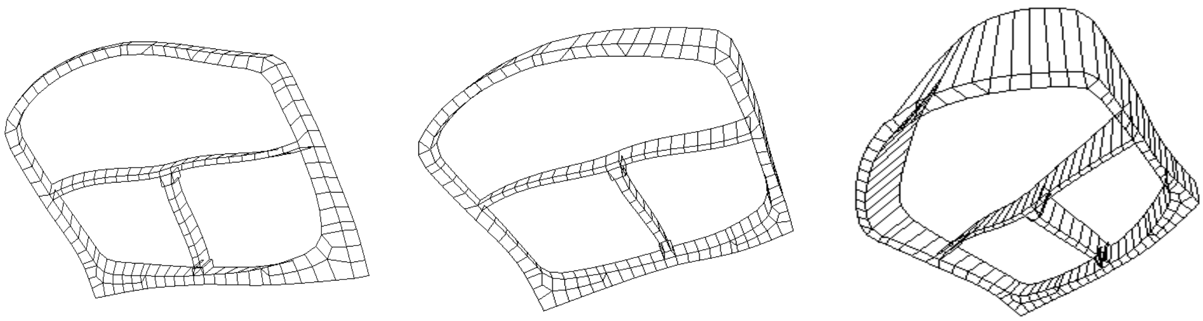

(**a**) 0.15 g (prefabricated) (**b**) 0.25 g (prefabricated) (**c**) 0.4 g (prefabricated)

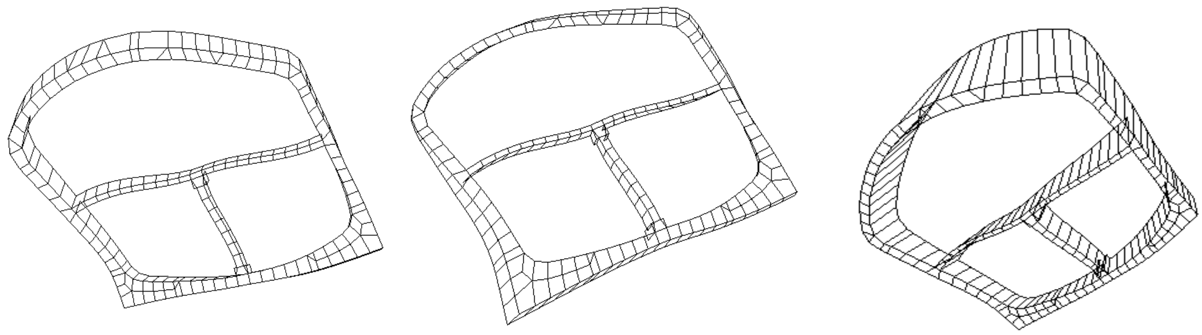

(**d**) 0.15 g (cast-in-place) (**e**) 0.25 g (cast-in-place) (**f**) 0.4 g (cast-in-place)

Figure 21. Station structure deformation diagram (500 times).

Under the 0.15 g ground shaking, the difference between the floating amount on both sides of the structural floor under the prefabricated condition and the cast-in-place condition is 8.10 mm and 11.69 mm, respectively. Under the 0.25 g ground shaking, the difference between the two floating amounts is 13.04 mm and 14.66 mm, respectively. Under the 0.4 g ground shaking, the difference between the two floating amounts is 32.53 mm and 32.88 mm, respectively. The difference in the floating amount between the left and right sides of the two structures after the end of the excitation increases with the increase in the intensity of the ground shaking. Comparing the difference in floating between the two structures, the PSSS has a lower difference in floating. This indicates that the PSSS has a better ability to resist overturning. This is due to the fact that the prefabricated structure is made of tongue-and-groove joints, and its flexible connection is easier to adapt to a larger vertical deformation than rigid connection. This phenomenon can also be visualized from the deformation diagrams of the two structures in Figure 21.

6. Conclusions

Based on the engineering background of Changchun Metro Line 2 Shuangfeng Station, a numerical analysis model of a liquefiable strata–prefabricated subway station structure (PSSS) interaction is established. The results of the seismic effects of the PSSS and cast-in-place structure are compared. Seismic response laws such as foundation pore water pressure, dynamic response of underground structure, floating characteristics of underground structure, and deformation characteristics of the PSSS are studied. The main conclusions are as follows:

(1) Similar to the cast-in-place condition, the excess pore pressure ratio at each monitoring point at the same depth in the condition of the PSSS in the liquefiable site also shows a development course of "slow increase at the beginning, followed by a rapid increase and finally stabilized". Under different intensities of ground shaking, there is little difference in the pore pressure effects of the two structures on the surrounding liquefiable soils. The PSSS can be constructed in a liquefiable site under the premise of ensuring static waterproofing.

(2) The underground structure provides some isolation of the surface acceleration response. When inputting a lower-intensity ground motion (0.15 g), the peak surface acceleration of the prefabricated station condition is slightly larger than that of the cast-in-place condition, especially at the measurement point directly above the station structure. When a higher-intensity ground motion (0.25 g and above) is input, the difference in the surface acceleration between the two conditions is not significant and the acceleration response of the liquefiable site soil in the two conditions is also closer.

(3) The dynamic properties of the PSSS remain suppressed under the constraints of the surrounding strata, providing better adaptation to ground deformation. The deformation of the upper part of the PSSS is slightly larger than that of the lower part, which is an important part of its deformation control. And the middle part is the key part of its strength control because of the existence of the center plate, which leads to the obvious increase in stiffness and stress.

(4) The higher the intensity of ground shaking, the shorter the time for the PSSS to reach the peak floating amount. The deformation of the PSSS under horizontal ground motion is closer to shear deformation. The flexible connection of the PSSS is easier to adapt to a larger vertical deformation than the rigid connection, and its ability to resist overturning is better.

Author Contributions: Conceptualization, J.A.; methodology, J.A.; software, Q.L.; formal analysis, Y.Z.; writing—original draft preparation, Q.L.; writing—review and editing, J.A. and X.Z.; supervision, J.A. and X.Z.; project administration, X.Z. All authors have read and agreed to the published version of the manuscript.

Funding: This work has been supported by the Fund of Colleges and Universities in Hebei province Science and Technology Research Project (QN2023079).

Data Availability Statement: The data presented in this study are available in the article.

Conflicts of Interest: The authors declare no conflict of interest.

References

1. Wang, L.; Chen, X.; Su, D. Mechanical performance of a prefabricated subway station structure constructed by twin closely-spaced rectangular pipe-jacking boxes. *Tunn. Undergr. Space Technol. Inc. Trenchless Technol. Res.* **2023**, *135*, 105062. [CrossRef]
2. Yang, X. Theory and Application of Prefabricated Open-Cut Metro Station Structure. Ph.D. Thesis, Beijing Jiaotong University, Beijing, China, 2020.
3. Tao, L.; Shi, C.; Ding, P. Shaking table test of the effect of an enclosure structure on the seismic performance of a prefabricated subway station. *Tunn. Undergr. Space Technol.* **2022**, *125*, 104533. [CrossRef]
4. Liu, H.; Wang, Z.; Du, X. The seismic behaviour of precast concrete interior joints with different connection methods in assembled monolithic subway station. *Eng. Struct.* **2021**, *232*, 111799. [CrossRef]
5. Du, X.; Liu, H.; Lu, D. Study on seismic performance of sidewall joints in assembled monolithic subway station. *China Civ. Eng. J.* **2017**, *50*, 38–47.
6. Ding, P.; Tao, L.; Yang, X. Three-dimensional Dynamic Response Analysis of a Single-Ring Structure in a Prefabricated Subway Station. *Sustain. Cities Soc.* **2019**, *45*, 271–286. [CrossRef]
7. Tao, L.; Cao, Q.C.; Shi, C. Seismic Responses of Prefabricated Metro Stations Built at Different Sites. *Tunn. Constr.* **2022**, *42*, 378–387.
8. Jiang, Z.; Yang, X.; Li, X. Response Comparisons of Precast and Cast-in-situ Subway Station Structures in the High Seismic Intensity Regione. *Eng. Mech.* **2023**. [CrossRef]
9. Wu, F. Research on Seismic Performance of Fully Prefabricated Subway Station Structure Based on Mortise and Groove Grouting Joint. Master's Thesis, Beijing Jiaotong University, Beijing, China, 2019.
10. Chen, J.; Xu, C.; Du, X.; Han, R.; El Naggar, H.M. Physical and numerical modeling of seismic soil-structure interaction of prefabricated subway station structure. *Eng. Struct.* **2023**, *290*, 116364. [CrossRef]
11. Chen, J.; Xu, C.; El Naggar, H.M.; Du, X. Quantification of seismic performance index limits and evaluation of seismic fragility for a new rectangular prefabricated subway station structure. *Tunn. Undergr. Space Technol.* **2023**, *138*, 105183. [CrossRef]
12. Wu, C.; Lu, D.; Ma, C.; El Naggar, M.H.; Du, X. Structural design and seismic performance analysis of partially prefabricated subway station structure. *Tunn. Undergr. Space Technol.* **2023**, *140*, 105264. [CrossRef]
13. Lingvay, I.; Bors, A.; Lingvay, D.; Ladislau, R.; Neagu, V. Electromagnetic Pollution of the Environment and its Effects on the Materials from the Built up Media. *Rev. De Chim.* **2019**, *69*, 3593–3599. [CrossRef]
14. Yan, G.; Xu, C.; Zhang, Z. Influence of soil-structure interface characteristics on seismic response of underground structure in the local liquefaction interlayer site. *Chin. J. Rock Mech. Eng.* **2023**, *42*, 3643–3653.
15. Cheng, K.; Miao, Y.; Peng, T. Experimental investigation on the effects of loess content on the liquefaction behavior of Taiyuan sand. *J. Huazhong Univ. Sci. Technol. (Nat. Sci. Ed.)* **2020**, *48*, 83–87.
16. Liu, C. Shaking Table Test on Influence of Liquefiable Soil Distribution on Seismic Response of Soil and Subway Underground Structures. *China Railw. Sci.* **2021**, *42*, 30–40.
17. An, J.; Yan, H.; Zhao, Z. Seismic response analysis of liquefiable soil layer on subway station structure. *Sci. Technol. Eng.* **2022**, *22*, 7080–7088.
18. Wang, K. Seismic Vulnerability Analysis of Assembled Subway Underground Station Structure. Master's Thesis, Xi'an Technological University, Xi'an, China, 2023.
19. Yang, X. Development and prospect of construction technology for prefabricated metro station in China. *Tunn. Constr.* **2021**, *41*, 1849.